Chapter 7
Magneto-Acoustic Hybrid Micro-/Nanorobot

Simon W. Sanchez and Jinxing Li

Future medical micro-/nanorobotics should be able to achieve efficient propulsion in harsh and complicated environments [1–12]. To do so, the micro-/nanorobotics need to harvest propelling forces with extremely high temporospatial resolution. Particularly, it is highly desired that micro-/nanorobotics are powered using biocompatible energy sources. Recently, the chemically powered micromotors have achieved a great success by showing the capacity to enable active and prolonged medicine delivery in living animals toward enhanced therapeutic efficacy [13–15]. Since these micromotors are mostly using onboard energy sources (Mg or Zn which can react with gastric or intestinal fluids), their lifetime is relatively short while the control and navigation have still not been explored in vivo. Alternatively, extensive efforts have been directed to the development of biocompatible fuel-free propulsion mechanisms [16–31]. Externally physical fields using optical, acoustic, or magnetic stimuli lead powerful navigation and actuation of micro-/nanorobotics. Expanding the capabilities and sophistication of such fuel-free nanomotors is imperative to design advanced micro-/nanorobotics for diverse biomedical applications (Fig. 7.1).

Among the various external fields, magnetic and acoustic fields play important roles in modern medicine. Magnetics are used in instruments such as the magnetic resonance imaging (MRI) machine, while transcranial magnetic stimulation (TMS) has shown diagnostic and therapeutic potential in the central nervous system with a wide variety of disease states in neurology and mental health. Acoustic fields with low amplitudes have been used for diagnostics and imaging. Meanwhile, many therapies use high-energy ultrasound for heating, activating, and fracturing tissues and structures within the body. Owing to their biocompatible energy transduction mechanism, magnetic and ultrasound propulsions have also led the operation of fuel-free nanomotors and hold considerable promise for biomedical applications, particularly in vivo ones.

Note: Results of this chapter are mainly based on the work published in: Li et al. Nano Lett. 2015, 15, 7, 4814–4821; and Ahmed et al. Nature Commun. 2017, 8, 770.

S. W. Sanchez · J. Li (✉)
Department of Biomedical Engineering & Institute for Quantitative Health Science & Engineering, Michigan State University, East Lansing, MI, USA
e-mail: jl@msu.edu

Y. Sun et al. (eds.), *Field-Driven Micro and Nanorobots for Biology and Medicine*, https://doi.org/10.1007/978-3-030-80197-7_7

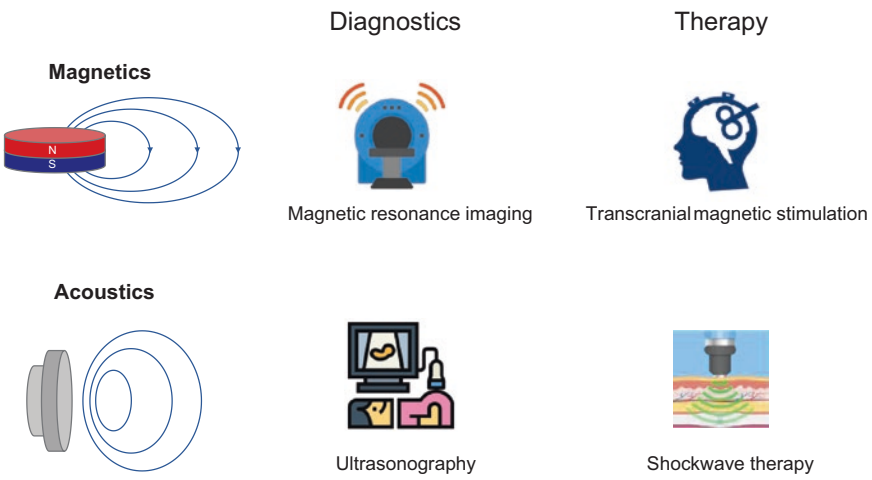

Fig. 7.1 Examples of magnetics and acoustics in modern medicine

Hybrid micro-/nanorobots, which use multiple distinct power sources for nanoscale propulsion, could lead to complex regulation of individual and collective behavior for operation in complicated environments. Hybrid nanomotors pairing fuel-powered and fuel-free propulsions in a single nanovehicle have been described recently by Wang's and Mallouk's groups [32–34]. Meanwhile, because of the high versatility and maneuverability of magnetic and acoustic fields for fuel-free operation, magneto-acoustic hybrid micro-/nanorobotics recently emerged as a valuable option for the digitalized speed regulation and reversible control of micro-/nanorobots.

The individual operation mode of magnetic and acoustic propulsion is briefly summarized in Fig. 7.2. Magnetic microrobot can mimic the helical or flexible flagellum of bacteria propulsion using either a rotational or an oscillating magnetic field. The motion of helical microswimmers is explained by slender body theory [16, 35–37], which approximates the helical structure as a slender filament by a line distribution of singularity solutions [38, 39]. For steady-state motion, the externally applied forces and torques have to equal the drag on the swimmer. This is like how a corkscrew being driven through wood rotationally with a screwdriver when the resistance is too large. Quite a few designs have been explored for undulatory magnetic propulsion using oscillating magnetic fields, including multi-linked nanoswimmers [40] and two-arm freestyle nanoswimmers [41]. Soft magnetic materials or ferrofluid droplets have recently been used to build shape-programmable magnetic miniature soft robots with attractive performance and reconfigurable actuation [42–44]. The acoustic propulsion is even more complicated and versatile. Standing waves, generated in resonant cavities, allow manipulation of objects by trapping them in the acoustic nodes [45]. Recently, such acoustic manipulation has been applied to precisely control a single microparticle/cell/organism along an arbitrary path within a single-layer microfluidic channel in two dimensions [46]. Steady

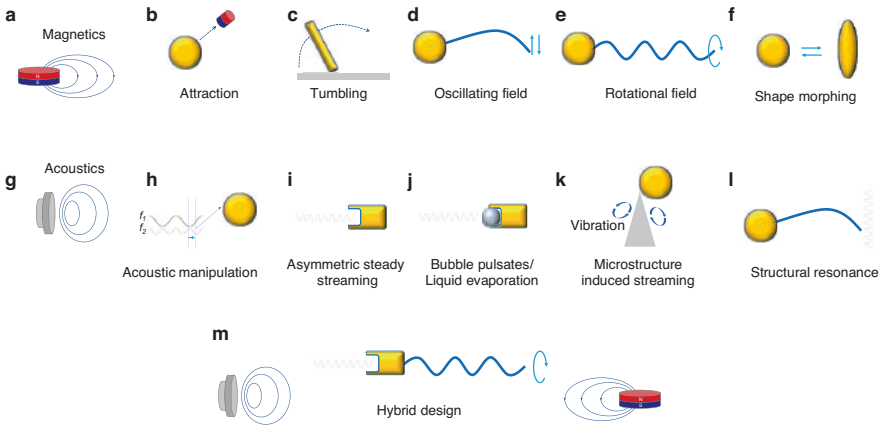

Fig. 7.2 Magnetic and acoustic actuation modes for hybrid design. (**a**) Magnetic actuation modes including (**b**) direct magnetic attraction of magnetic structures; (**c**) magnetic structure tumbling on a surface; (**d**) undulatory magnetic actuation using oscillating magnetic field; (**e**) helical magnetic actuation under a rotational magnetic field; (**f**) shape-morphing microrobot induced by magnetic field. (**g**) Acoustic actuation modes including (**h**) acoustic manipulation by switching operation frequency; (**i**) "self-propelled" motion induced by asymmetry steady streaming; (**j**) acoustic field induced bubble pulsation or liquid evaporation in a microcavity; (**k**) nanomanipulation by streaming induced by local microstructures; (**l**) structure resonance of a soft nanostructure; (**m**) an example of magneto-acoustic hybrid nanorobot combing the asymmetric stead streaming and the helical actuation

streaming around obstacles in an acoustically induced flow, either standing wave or traveling wave, can also be used to trap and precisely manipulate micro-/nanoscale objects [47, 48]. Recently, Fischer et al. demonstrated that 3D-printed surface profile encoding the phase of the desired wave front can shape acoustic fields to be used as reflection elements in air to levitate dense solids and liquids within complex traps [49]. Recent experiments from the Mallouk and Wang groups also showed that standing acoustic waves are highly promising to induce the self-prolusion of rigid metallic structures in the direction perpendicular to the acoustic wave [20, 21]. The physical mechanism for such new actuation modes is assumed to be based on the interplay between inertial forces in the fluid and the geometrical asymmetry of the particle shape [50]. Steady streaming in the fluid, the inertial rectification of the time-periodic oscillating flow, generates steady stresses on the particle which, in general, do not average to zero, resulting in a finite propulsion speed along the axis of the symmetry of the particle and perpendicular to the oscillation direction [50]. Microstructure trapping air bubble can harness acoustic waves for propulsion at incredibly high speeds [51], while microstructure loaded with liquid that evaporates under focused ultrasound can lead a one-time high-speed shot to penetrate the biological tissue [52]. Recently, Nelson et al. described a new class of nanoswimmer propelled by the small-amplitude oscillation of a flagellum-like flexible tail in both standing and traveling acoustic waves [53]. Different from the rigid asymmetric microstructures, the artificial nanoswimmers are fabricated by multistep

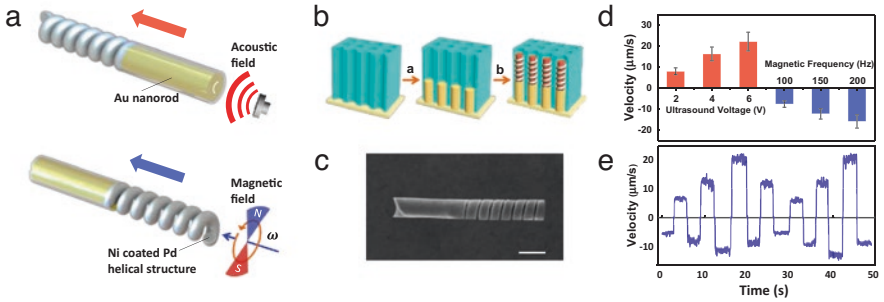

Fig. 7.3 (**a**) Scheme of the design of the magneto-acoustic hybrid nanomotor and its dual propulsion modes under the acoustic and magnetic fields. (**b**) Schematic illustration of the template-assisted fabrication of the bi-segment magneto-acoustic hybrid nanomotors. (**c**) SEM image of a magneto-acoustic hybrid nanomotor. Scale bar: 500 nm. (**d**) Quantitative velocity of the hybrid motor using magnetic frequencies of 100 Hz, 150 Hz, and 200 Hz and ultrasound voltage amplitudes of 2 V, 4 V, and 6 V (number of tracked nanomotors; $N = 20$). All the speed data are averaged by 20 nanomotors under the same propulsion conditions. (**e**) Digital control of the hybrid motor speed by changing the actuation mode and the corresponding ultrasound voltage and rotational magnetic frequency alternately every 3 seconds using the following sequence: Mag 100 Hz, US 2 V, Mag 150 Hz, US 4 V, Mag 200 Hz, US 6 V, Mag 150 Hz, US 4 V, Mag 100 Hz, US 2 V, Mag 150 Hz, US 4 V, Mag 200 Hz, US 6 V, Mag 150 Hz

electrodeposition techniques, compromising a rigid bimetallic head and a flexible tail. The flexibility of the tail structures allows high-frequency oscillation during the acoustic excitation, which produce high propulsive forces.

As one can see from the above summary, the many modalities to use magnetic and acoustic fields for micro-/nanorobotic propulsion open the many opportunities to develop magneto-acoustic hybrid micro-/nanorobotics. Li et al. describe the magneto-acoustic hybrid fuel-free nanomotor which can be powered by either a magnetic or ultrasound field [54]. To address the challenge of using the propulsion force from both magnetic and acoustic fields, the hybrid nanomotor is constructed from bi-segment nanomechanical elements, where a concave nanorod segment is essential to produce the asymmetric interplay between the nanostructure and the acoustic wave. Such concave end is connected to a nanohelical magnetic segment which was realized through a versatile template-assisted electrochemical deposition method followed by segment-selective chemical etching (Fig. 7.3b). The resulting nanostructures offer an impressive fuel-free magneto-acoustic hybrid nanomotor operation with the magnetic helical end serving for the magnetic propulsion and the concave nanorod for acoustic propulsion (Fig. 7.3a, bottom and top, respectively). The magneto-acoustic hybrid nanomotors can thus be powered by either the magnetic or ultrasound field and change their direction instantaneously upon alternating the applied fields. Changing the amplitude of the acoustic field or the frequency of the magnetic field leads to rapid speed regulation of such hybrid nanomotors.

Precise speed control of the hybrid nanomotor was achieved using an ultrasonic transducer at a resonant frequency of 2.66 MHz and two orthogonal Helmholtz coil pairs creating a rotational magnetic field frequency of 150 Hz. The hybrid

nanomotor was proven to move in opposite directions along the nanowire axis under the dual modes using an external magnet for alignment. Under the magnetic mode, the hybrid nanomotor moves "forward" toward its Au end. Similarly, under the acoustic mode, the hybrid nanomotor moves "backward" toward its helical end. Brownian motion is observed in the absence of both acoustic and magnetic fields. Dynamic speed changes as well as the ability to repeatedly move in opposite directions illustrate the rapid response of the hybrid nanomotor to different external stimuli. Overall, the hybrid nanomotor offers an on-demand operation and direction switching with steady-state speeds.

The speed of chemically powered nanomotors can be controlled by parameters of the chemical environment, such as fuel concentration and temperature [55]. However, real-time and rapid speed regulation is still challenging for chemical-powered nanomotors. Since the hybrid nanomotor is completely fuel-free and powered by external fields, its speed could be controlled by changing the input parameters of the corresponding field. Under acoustic mode, a nanoparticle can be viewed as a body oscillating in a uniform oscillating velocity field [50]. Based on the physical mechanism of asymmetric steady fluid streaming, the inertial rectification of the time-periodic oscillating flow generates steady stresses on the nanomotor which, in general, do not average to zero, resulting in a finite propulsion speed along the axis of the symmetry of the particle and perpendicular to the oscillation direction. The dimensional propulsion speed of the nanomotor can be expressed as [50]:

$$v_u = \varepsilon R_e V^{\perp} v^{(1,1)} \tag{7.1}$$

where ε is the dimensionless small shape parameter, R_e is the Reynolds number, $v^{(1,1)}$ is the leading-order dimensionless propulsion speed, and $V^{\perp}$ is the relative amplitude of the particle oscillations which scales with the amplitude of the ultrasound field. Therefore, the speed of the hybrid nanomotors levitated in solution under a fixed ultrasound wave frequency can be readily controlled by changing the amplitude of the driving voltage.

The speed of helical magnetic swimmers depends upon various geometric parameters (including the diameter) and the rotation frequency, in a complex manner described in Eq. 7.2 [56, 57]:

$$v_u = \frac{\left(\xi_{\perp} - \xi_{\parallel}\right)\sin\theta\cos\theta}{2\left(\xi_{\perp}\sin^2\theta + \xi_{\parallel}\cos^2\theta\right)} dw \tag{7.2}$$

where $\xi_{\perp}$ and $\xi_{\parallel}$are the drag coefficients perpendicular and parallel to the helical axis, θ is the helix angle, d is diameter of the helix, and ω is the rotational frequency. Therefore, the speed of the hybrid nanomotor in a certain fluid, operated in the magnetic mode, can be regulated by controlling the rotational frequency of the magnetic field. Overall, the speed of the new hybrid motor under the magnetic and ultrasound actuations could be controlled by controlling the rotation frequency of the magnetic field and the voltage amplitude applied on the piezoelectric transducer, respectively.

The propulsion performance was tested using different input parameters of the individual modes. In the acoustic mode, the applied voltage was increased from 2 to 4 to 6 with an observed speed increase from 8.1 to 16.4 to 22.3 μm/s, respectively, over 4 s periods in agreement with Eq. 7.1. Similarly, in the magnetic mode, the rotational frequency was increased from 100 to 150 to 200 Hz with an observed speed increase from 7.6 to 12.3 to 15.9 μm/s, respectively (Fig. 7.3d). A net speed of zero and an equilibrium state could be achieved by adjusting the ultrasound and magnetic propelling forces to be balanced. Overall, the data follows the theoretical predictions of Eqs. 7.1 and 7.2. The hybrid motor displayed rapid switching of its propulsion modes upon applying the corresponding actuation, a characteristic of an ideal hybrid motor. This capability was achieved by alternating the magnetic and acoustic fields (every 3 s) while also changing the corresponding ultrasound voltage and rotational magnetic frequency. The hybrid motor displayed an instantaneous switching between its dual modes with steady-state speeds increasing rapidly upon changing the input parameters. Careful analysis indicates that the hybrid motor can reverse its moving direction within less than 50 ms (Fig. 7.3e). In conclusion, rapid, on-demand, and programmable speed and direction control are achievable with the combination of acoustic and magnetic fields.

In order to test the critical role of the bi-segment configuration for optimal hybrid propulsion in both modes, the hybrid motor with that of its individual segments, an Au nanorod or a Pd nanospring (both coated with 10-nm Ni thin layer), was also tested. The results demonstrate that the magnetic nanospring structure can still lead to a useful hybrid operation. However, the hybrid spring-rod nanomotors can harvest and translate the propelled forces more efficiently. Overall, the bi-segment nanowire design of the hybrid nanomotor does not compromise the performance of the individual propulsion modes.

For practical biomedical applications of the new hybrid nanomotors, it is important to test their propulsion behavior in different complex environments. It was observed that magneto-acoustic hybrid nanomotors exhibit slower speed in biological medium such as serum and blood. These changes reflect the increased environmental viscosity of these biofluids. Chemically powered nanomotors cannot operate in high ionic strength environments (such as seawater and blood) because these media interfere with their self-electrophoresis propulsion mechanism. While these environments affect the speed of the hybrid nanomotors, these motors still move efficiently in both modes in the different viscous fluids.

Collective behavior, a very common phenomenon in the biological world [58], inspired us to investigate how groups of the hybrid motors behave under the external field inputs. The acoustic field (frequency 618 kHz) is capable to trigger the standing wave formation which leads to the rapid assembly and aggregation of the hybrid nanomotors toward the acoustic field node. In contrast, the magnetic actuation induces disassembly of the aggregate hybrid motors and directs the directional motion of the nanomotor swarm. Such reversible assembly and directional swarm movement is achieved by alternating the acoustic and magnetic fields. This switchable collective behavior can be repeated with multiple cycles. Thus, with proper application of the acoustic and magnetic fields, a fully reversible swarm with

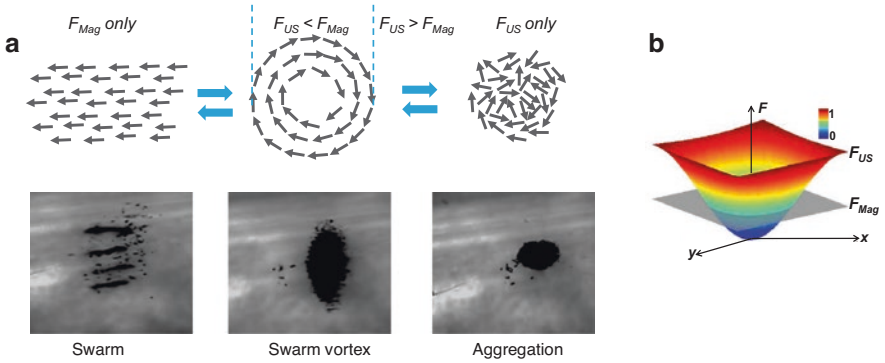

Fig. 7.4 (**a**) Illustration of swarm vortex formation in a round boundary system: The hybrid nanomotors display directional swarm motion when only the magnetic field is "on"; rapid re-formation of the swarm vortex upon turning the ultrasound field "on" again; a stable aggregation is formed when only the ultrasound field is turned "on." (**b**) Normalized distribution of the acoustic force gradient F_{us} and magnetic force F_{mag} near the ultrasound pressure node in the acoustic cell. The magnetic force is considered to have a uniform distribution, shown by the gray plane

aggregation and dispersion of the nanomotors can be obtained. It is anticipated that the nanomotor swarm can be moved in a controlled way by varying the applied acoustic frequency which changes the location of the pressure nodes and leads to migration of the swarm to a new location.

The collective behavior of hybrid nanomotors in the presence of both the acoustic and magnetic fields (i.e., a "dual operation mode") is particularly intriguing as three distinct states are observed (Fig. 7.4). Interestingly, unlike the directional swarm motion observed under the magnetic field alone or the stable aggregation under the acoustic field, a swarm vortex is formed when both of the fields are turned "on." Turning the acoustic field "off" in such a state leads to directional moving swarm of the nanomotors under the rotational magnetic field. Applying the acoustic field again leads to rapid migration of the hybrid motors toward the original node position and re-formation of a swarm vortex, although the magnetic field is still "on." Upon removal of the magnetic field, the acoustic field prevails, and a stable assembly is formed again. The three different states of the swarm vortex (when both fields "on"), directional swarm motion (only the Mag is "on"), and the stable assembly (only the US "on") are highly switchable and reversible (Fig. 7.4a).

Such flexible switching of the collective behavior results from the competition between the magnetic and acoustic forces. At steady state, the imposed propelling force is always counterbalanced by the Stokes drag force. From Eq. 7.2, one can note that the magnetic propelling force imposed on a hybrid nanomotor is always consistent at a fixed frequency. Under the acoustic actuation with a frequency of 618 kHz, a plane standing wave field arises from the superposition of two waves (one is generated by the transducer, while the other is reflected by the cover slide) of equal wavelength and amplitude traveling in opposite directions. The interference between the waves results in the formation of antinodes and nodes, with zero

levitation force at the pressure nodes. The acoustic force can be divided into the primary radiation force (PRF) and the secondary radiation force (SRF). The PRF, which is the main force in the field of acoustic waves, can be subdivided into an axial component F_z and a transverse component F_{xy} [59, 60]. The F_z component of the PRF is the force that drives the migration of microparticles to the nearest pressure node or antinode plane, while the F_{xy} component leads to their aggregation within the nodal plane. The experiment depends on the theoretical understanding of the F_z component of the PRF which drives the nanomotor in a standing ultrasound wave field [59, 60].

$$F_z = VE_{\text{ac}} \frac{2\pi}{\lambda} Q \sin\left(\frac{4\pi}{\lambda} z\right) \tag{7.3}$$

Here V is the nanomotor volume, z is the axial distance from the transducer to the node or antinode plane, λ is the wavelength, and Q is the acoustic contrast factor which is related to the particle fluid interactions. The acoustic energy density E_{ac} is equal to the sum of the average potential and kinetic energy densities. As indicated from Eq. 7.3, the acoustic force exhibits a sinusoidal dependence of the axial distance from the transducer to the node or antinode plane. Therefore, the acoustic force drops rapidly near the node and becomes zero at the node (Fig. 7.4b). In this case, within a certain distance from the node position, the magnetic propelling force is larger than the acoustic radiation force. Once the nanomotor approaches the equilibrium round boundary where the magnetic and acoustic forces become equal, the nanomotors can no longer achieve directional motion, and instead aggregate rapidly into a swarm vortex configuration with zero density in the center. Since the ultrasound radiation force boundaries are reflecting, the velocity perpendicular to the boundary is suppressed in the course of collisions with other nanomotors on the way back from the boundary [61]. As a consequence, the velocity parallel to the wall survives and becomes a natural attractor for the dynamics. The circular system boundaries conform perfectly to parallel velocity, resulting in a tight vortex formation. At the position beyond the equilibrium boundary, the increased acoustic force will dominate the motion of the nanomotor and tow the nanomotor again toward the node position. Further aggregation with magnetic field off is facilitated by the SRF, which is associated with the sound waves that are scattered by individual nanomotors. The SRF is responsible for particle-particle interactions, making them either to attract or repel each other, as well as forming stable multiparticle spherical structures [59, 60]. Such diverse and unique collective behaviors, e.g., vortex formation and swarm motion, of the hybrid nanomotor system, can serve as a good model for complex open systems such as bacterial chemotaxis or cell migrations [61, 62].

The biocompatible and versatile propulsion enabled by the hybridization of magnetic and acoustic fields leads to great potential for actuation in complex biological structures and environments. Specifically, controlled propulsion within vascular environments offers exciting possibilities to access the whole body and to provide localized treatments for cardiovascular diseases. Precise control and motion of

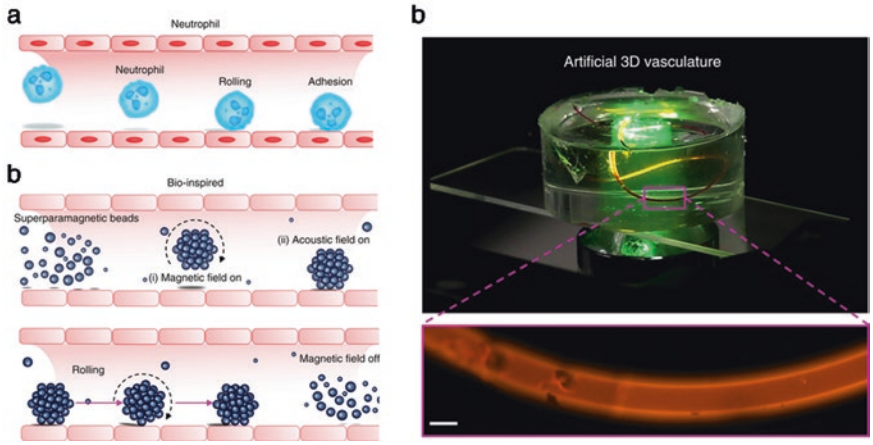

Fig. 7.5 Magneto-acoustic neutrophil-inspired microrobots [63]. (**a**) Neutrophil rolls on vasculature before transmigrating into tissue. (**b**) Hybridization of magnetic and acoustic propulsion leads to three-dimensional control motion of reconfigurable particle assembles moving a vessel wall mimicking a neutrophil rolling on a wall. (**c**) A three-dimensional PDMS-based artificial vasculature which can be navigated through by the magneto-acoustic neutrophil-inspired microrobots

micro- or nanoswimmers provide a pathway for targeted therapeutics and noninvasive surgery. Moving and navigation in such complicated environment requires propulsion mechanisms beyond two-dimensional settings with limited control at the boundaries. Ahmed et al. show a mechanism in which to use micro-sized particles in a microvascular environment that are capable to be propelled by the combination of magnetic and acoustic fields [63]. Such hybridization of magnetic and acoustic propulsion leads to three-dimensional control motion of reconfigurable particle assemblies moving along vessel wall mimicking a neutrophil rolling on a wall (Fig. 7.5a). A rolling motion is achieved by using micro-sized superparamagnetic particles in a channel after a rotational magnetic field is applied (Fig. 7.5b). The aggregations are formed due to the dipole-dipole interactions. When an acoustic field with an appropriate frequency is applied, the assembled particles migrate to the boundary in an acoustic field which resulted in a rolling motion along vessel wall. The assembled particles become dispersed again when the magnetic field is off.

Using a polydimethylsiloxane (PDMS)-based microchannel as the artificial vasculature system (Fig. 7.5c), the authors investigated the migration of the particles toward the sidewall of the channel by using various sized particles of different material properties. There are several acoustic forces that can contribute to particle motion including acoustic radiation force and the streaming-induced drag. Of the acoustic radiation force, there are the primary and secondary radiation forces. The primary radiation force was observed to mainly contribute to migration. For small particles, the sidewall-induced streaming drag force dominates particle motion until a certain size is met then which the radiation force becomes dominant. This work illustrates a mechanism in which superparamagnetic particles self-aggregate and

move along a boundary of a microchannel with a combined acoustic and magnetic actuation technique. This mechanism provides a foundation site-specific drug delivery and various other biomedical applications. The combined propulsion mechanism with a high-resolution imaging technique for in vivo treatment could provide a way to treat various diseases in hard-to-reach locations. The biocompatible magnetic particles are advantageous over already established microswimmers with costly fabrication procedures and limited biocompatibility.

The use of the combination of magnetic and acoustic fields to power a hybrid device offers a wider scope of operation and holds substantial promise for designing smart nanovehicles that autonomously adapt and reconfigure their operation in response to changes in their surrounding environment. Addressing the distinct requirements of the magnetic and acoustic propulsions within a single nanoscale device requires high-precision fabrication techniques to make structures that can harvest both the magnetic and acoustic forces. The resulting hybrid nanomotor can take advantage of the propelling forces from both magnetic and acoustic fields for efficient fuel-free dual-mode hybrid motor operation. The speed and directionality of the hybrid nanomotors can be swiftly controlled by changing the parameters of the field inputs. The hybrid nanomotors can also achieve efficient propulsion in biological media and demonstrate impressive switchable collective behaviors. Dynamic and reversible change between a tight assembly, swarm motion, and swarm vortex state can be achieved in response to a change of the acoustic and/or magnetic actuations. Such multimode fuel-free propulsion capability offers a wider scope of operation and substantial promise for adaptive performance under various scenarios in dynamically changing environments. Such adaptive and hybrid operation provide a versatile route to precisely control a single or a large number of nanomotors which could not be achieved by using only one propulsion mode.

Overall, the magneto-acoustic hybrid nanomotors can function individually and collectively, with rapid switching between the magnetic and acoustic modes and precise temporal-spatial control and regulation. Future efforts will lead to intelligent hybrid vehicles to be coupled with conventional magnetic and ultrasound diagnostic devices with real-time autonomous mode switching in response to changing conditions. Meanwhile, various medical functions, such as imaging and drug delivery, could be integrated on the nanomotors for multitask response and operation. Owing to their impressive performance, the new hybrid magneto-acoustic nanomotors are expected to advance the field of artificial nanomachines and to offer considerable promise for a broad range of practical applications ranging from nanoscale manipulation to nanomedicine. Beyond hybrid actuation, researchers should also take advantage of the imaging functions of magnetics and acoustics to eventually achieve four-dimensional control and navigation of individual microrobot or a swarm of micro-/nanorobots in body, so that the “fantastic voyage” can be realized.

References

1. Purcell, E. M. (1977). Life at low Reynolds number. *American Journal of Physics, 45*, 3–11.
2. Schliwa, M., & Woehlke, G. (2003). Molecular motors. *Nature, 422*, 759–765.
3. van den Heuvel, M. G. L., & Dekker, C. (2007). Motor proteins at work for nanotechnology. *Science, 317*, 333–336.
4. Guix, M., Mayorga-Martinez, C. C., & Merkoçi, A. (2014). Nano/micromotors in (bio)chemical science applications. *Chemical Reviews, 114*, 6285–6322.
5. Ozin, G. A., Manners, I., Fournier-Bidoz, S., & Arsenault, A. (2005). Dream nanomachines. *Advanced Materials, 17*, 3011–3018.
6. Wang, J. (2013). *Nanomachines: Fundamentals and applications*. Wiley-VCH.
7. Mei, Y., Solovev, A. A., Sanchez, S., & Schmidt, O. G. (2011). Rolled-up nanotech on polymers: From basic perception to self-propelled catalytic microengines. *Chemical Society Reviews, 40*, 2109–2119.
8. Mallouk, T. E., & Sen, A. (2009). Powering nanorobots. *Scientific American, 300*, 72–77.
9. Nelson, B. J., Kaliakatsos, I. K., & Abbott, J. J. (2010). Microrobots for minimally invasive medicine. *Annual Review of Biomedical Engineering, 12*, 55–85.
10. Moo, J. G. S., & Pumera, M. (2015). Chemical energy powered nano/micro/macromotors and the environment. *Chemistry – A European Journal, 21*, 58–72.
11. Li, J., de Ávila, B. E.-F., Gao, W., Zhang, L., & Wang, J. (2017). Micro/nanorobots for biomedicine: Delivery, surgery, sensing, and detoxification. *Science Robotics, 2*.
12. Alapan, Y., et al. (2019). Microrobotics and microorganisms: Biohybrid autonomous cellular robots. *Annual Review of Control, Robotics, and Autonomous Systems, 2*, 205–230.
13. Gao, W., et al. (2015). Artificial micromotors in the mouse's stomach: A step toward in vivo use of synthetic motors. *ACS Nano, 9*, 117–123.
14. Li, J., et al. (2016). Enteric micromotor can selectively position and spontaneously propel in the gastrointestinal tract. *ACS Nano, 10*, 9536–9542.
15. de Ávila, B. E.-F., et al. (2017). Micromotor-enabled active drug delivery for in vivo treatment of stomach infection. *Nature Communications, 8*, 272.
16. Dreyfus, R., et al. (2005). Microscopic artificial swimmers. *Nature, 437*, 862–865.
17. Liu, M., Zentgraf, T., Liu, Y., Bartal, G., & Zhang, X. (2010). Light-driven nanoscale plasmonic motors. *Nature Nanotechnology, 5*, 570–573.
18. Loget, G., & Kuhn, A. (2010). Propulsion of microobjects by dynamic bipolar self-regeneration. *Journal of the American Chemical Society, 132*, 15918–15919.
19. Chang, S. T., Paunov, V. N., Petsev, D. N., & Velev, O. D. (2007). Remotely powered self-propelling particles and micropumps based on miniature diodes. *Nature Materials, 6*, 235–240.
20. Wang, W., Castro, L. A., Hoyos, M., & Mallouk, T. E. (2012). Autonomous motion of metallic microrods propelled by ultrasound. *ACS Nano, 6*, 6122–6132.
21. Garcia-Gradilla, V., et al. (2013). Functionalized ultrasound-propelled magnetically guided nanomotors: Toward practical biomedical applications. *ACS Nano, 7*, 9232–9240.
22. Schamel, D., et al. (2014). Nanopropellers and their actuation in complex viscoelastic media. *ACS Nano, 8*, 8794–8801.
23. Qiu, T., et al. (2014). Swimming by reciprocal motion at low Reynolds number. *Nature Communications, 5*, 5119.
24. Venugopalan, P. L., et al. (2014). Conformal cytocompatible ferrite coatings facilitate the realization of a nanovoyager in human blood. *Nano Letters, 14*, 1968–1975.
25. Ghosh, A., & Fischer, P. (2009). Controlled propulsion of artificial magnetic nanostructured propellers. *Nano Letters, 9*, 2243–2245.
26. Wu, Z., et al. (2014). Turning erythrocytes into functional micromotors. *ACS Nano, 8*, 12041–12048.
27. Loget, G., & Kuhn, A. (2011). Electric field-induced chemical locomotion of conducting objects. *Nature Communications, 2*, 535.

28. Wu, Z., et al. (2014). Near-infrared light-triggered "on/off" motion of polymer multilayer rockets. *ACS Nano, 8*, 6097–6105.
29. Sridhar, V., et al. (2020). Carbon nitride-based light-driven microswimmers with intrinsic photocharging ability. *Proceedings of the National Academy of Sciences, 117*, 24748–24756.
30. Dong, X., et al. (2020). Bioinspired cilia arrays with programmable nonreciprocal motion and metachronal coordination. *Science Advances, 6*, eabc9323.
31. Palagi, S., et al. (2016). Structured light enables biomimetic swimming and versatile locomotion of photoresponsive soft microrobots. *Nature Materials, 15*, 647–653.
32. Gao, W., Manesh, K. M., Hua, J., Sattayasamitsathit, S., & Wang, J. (2011). Hybrid nanomotor: A catalytically/magnetically powered adaptive nanowire swimmer. *Small, 7*, 2047–2051.
33. Gao, W., D'Agostino, M., Garcia-Gradilla, V., Orozco, J., & Wang, J. (2013). Multi-fuel driven Janus micromotors. *Small, 9*, 467–471.
34. Wang, W., et al. (2014). A tale of two forces: Simultaneous chemical and acoustic propulsion of bimetallic micromotors. *Chemical Communications, 51*, 1020–1023.
35. Bell, D. J., Leutenegger, S., Hammar, K. M., Dong, L. X., & Nelson, B. J. (2007). Flagella-like propulsion for microrobots using a nanocoil and a rotating electromagnetic field. In *Proceedings 2007 IEEE international conference on robotics and automation* (pp. 1128–1133). https://doi.org/10.1109/ROBOT.2007.363136
36. Zhang, L., et al. (2009). Artificial bacterial flagella: Fabrication and magnetic control. *Applied Physics Letters, 94*, 064107.
37. Zhang, L., et al. (2009). Characterizing the swimming properties of artificial bacterial flagella. *Nano Letters, 9*, 3663–3667.
38. Lighthill, J. (1976). Flagellar hydrodynamics. *SIAM Review, 18*, 161–230.
39. Brennen, C., & Winet, H. (1977). Fluid mechanics of propulsion by cilia and flagella. *Annual Review of Fluid Mechanics, 9*, 339–398.
40. Jang, B., et al. (2015). Undulatory locomotion of magnetic multilink nanoswimmers. *Nano Letters, 15*, 4829–4833.
41. Li, T., et al. (2017). Highly efficient freestyle magnetic nanoswimmer. *Nano Letters, 17*, 5092–5098.
42. Fan, X., Dong, X., Karacakol, A. C., Xie, H., & Sitti, M. (2020). Reconfigurable multifunctional ferrofluid droplet robots. *Proceedings of the National Academy of Sciences, 117*, 27916–27926.
43. Kim, Y., Yuk, H., Zhao, R., Chester, S. A., & Zhao, X. (2018). Printing ferromagnetic domains for untethered fast-transforming soft materials. *Nature, 558*, 274–279.
44. Huang, H.-W., Sakar, M. S., Petruska, A. J., Pané, S., & Nelson, B. J. (2016). Soft micromachines with programmable motility and morphology. *Nature Communications, 7*, 12263.
45. Wixforth, A., et al. (2004). Acoustic manipulation of small droplets. *Analytical and Bioanalytical Chemistry, 379*, 982–991.
46. Ding, X., et al. (2012). On-chip manipulation of single microparticles, cells, and organisms using surface acoustic waves. *Proceedings of the National Academy of Sciences, 109*, 11105–11109.
47. Lu, X., et al. (2019). A human microrobot interface based on acoustic manipulation. *ACS Nano, 13*, 11443–11452.
48. Nama, N., Huang, P.-H., Huang, T. J., & Costanzo, F. (2014). Investigation of acoustic streaming patterns around oscillating sharp edges. *Lab on a Chip, 14*, 2824–2836.
49. Melde, K., Mark, A. G., Qiu, T., & Fischer, P. (2016). Holograms for acoustics. *Nature, 537*, 518–522.
50. Nadal, F., & Lauga, E. (2014). Asymmetric steady streaming as a mechanism for acoustic propulsion of rigid bodies. *Physics of Fluids, 26*, 082001.
51. Aghakhani, A., Yasa, O., Wrede, P., & Sitti, M. (2020). Acoustically powered surface-slipping mobile microrobots. *Proceedings of the National Academy of Sciences, 117*, 3469–3477.

52. Kagan, D., et al. (2012). Acoustic droplet vaporization and propulsion of perfluorocarbon-loaded microbullets for targeted tissue penetration and deformation. *Angewandte Chemie, International Edition, 51*, 7519–7522.
53. Ahmed, D., et al. (2016). Artificial swimmers propelled by acoustically activated flagella. *Nano Letters, 16*, 4968–4974.
54. Li, J., et al. (2015). Magneto-acoustic hybrid nanomotor. *Nano Letters, 15*, 4814–4821.
55. Wang, J., & Manesh, K. M. (2010). Motion control at the nanoscale. *Small, 6*, 338–345.
56. Tottori, S., et al. (2012). Magnetic helical micromachines: Fabrication, controlled swimming, and cargo transport. *Advanced Materials, 24*, 811–816.
57. Lauga, E., & Powers, T. R. (2009). The hydrodynamics of swimming microorganisms. *Reports on Progress in Physics, 72*, 096601.
58. Vicsek, T., & Zafeiris, A. (2012). Collective motion. *Physics Reports, 517*, 71–140.
59. Laurell, T., Petersson, F., & Nilsson, A. (2007). Chip integrated strategies for acoustic separation and manipulation of cells and particles. *Chemical Society Reviews, 36*, 492–506.
60. Xu, T., et al. (2015). Reversible swarming and separation of self-propelled chemically powered nanomotors under acoustic fields. *Journal of the American Chemical Society, 137*, 2163–2166.
61. Grossman, D., Aranson, I. S., & Jacob, E. B. (2008). Emergence of agent swarm migration and vortex formation through inelastic collisions. *New Journal of Physics, 10*, 023036.
62. Ingham, C. J., & Jacob, E. B. (2008). Swarming and complex pattern formation in Paenibacillus vortex studied by imaging and tracking cells. *BMC Microbiology, 8*, 36.
63. Ahmed, D., et al. (2017). Neutrophil-inspired propulsion in a combined acoustic and magnetic field. *Nature Communications, 8*, 770.